

## Highlights

### **Sampling Complex Topology Structures for Spiking Neural Networks**

Shen Yan, Qingyan Meng, Mingqing Xiao, Yisen Wang, Zhouchen Lin

- The SNN architectures significantly benefit from much more complex connection topologies
- Incorporating synaptic delay provides a novel perspective to the design of SNN architectures
- The novel sampling method greatly accelerates the process of obtaining SNN architectures

# Sampling Complex Topology Structures for Spiking Neural Networks

Shen Yan<sup>a</sup>, Qingyan Meng<sup>b,c</sup>, Mingqing Xiao<sup>d</sup>, Yisen Wang<sup>d,e</sup>, Zhouchen Lin<sup>d,e,f,\*</sup>

<sup>a</sup>*Center for Data Science, Peking University, China*

<sup>b</sup>*The Chinese University of Hong Kong, Shenzhen, China*

<sup>c</sup>*Shenzhen Research Institute of Big Data, Shenzhen 518115, China*

<sup>d</sup>*Key Lab of General AI, School of Intelligence Science and Technology, Peking University, China*

<sup>e</sup>*Institute for Artificial Intelligence, Peking University, China*

<sup>f</sup>*Peng Cheng Laboratory, Shenzhen, 518055, China*

---

## Abstract

Spiking Neural Networks (SNNs) have been considered a potential competitor to Artificial Neural Networks (ANNs) due to their high biological plausibility and energy efficiency. However, the architecture design of SNN has not been well studied. Previous studies either use ANN architectures or directly search for SNN architectures under a highly constrained search space. In this paper, we aim to introduce much more complex connection topologies to SNNs to further exploit the potential of SNN architectures. To this end, we propose the topology-aware search space, which is the first search space that enables a more diverse and flexible design for both the spatial and temporal topology of the SNN architecture. Then, to efficiently obtain

---

\*Corresponding author

*Email addresses:* [yanshen@pku.edu.cn](mailto:yanshen@pku.edu.cn) (Shen Yan), [qingyanmeng@link.cuhk.edu.cn](mailto:qingyanmeng@link.cuhk.edu.cn) (Qingyan Meng), [mingqing\\_xiao@pku.edu.cn](mailto:mingqing_xiao@pku.edu.cn) (Mingqing Xiao), [yisen.wang@pku.edu.cn](mailto:yisen.wang@pku.edu.cn) (Yisen Wang), [zlin@pku.edu.cn](mailto:zlin@pku.edu.cn) (Zhouchen Lin)

architecture from our search space, we propose the spatio-temporal topology sampling (STTS) algorithm. By leveraging the benefits of random sampling, STTS can yield powerful architecture without the need for an exhaustive search process, making it significantly more efficient than alternative search strategies. Extensive experiments on CIFAR-10, CIFAR-100, and ImageNet demonstrate the effectiveness of our method. Notably, we obtain 70.79% top-1 accuracy on ImageNet with only 4 time steps, 1.79% higher than the second best model.

*Keywords:*

spiking neural networks, neural architecture search

---

## 1. Introduction

Spiking Neural Networks (SNNs), regarded as the third generation of neural networks (Maass, 1997), have attracted considerable attention due to their energy efficiency and high biological plausibility (Lee et al., 2016; Shrestha  
5 and Orchard, 2018; Wu et al., 2018; Roy et al., 2019; Fang et al., 2021a; Xiao  
et al., 2021; Li et al., 2021). The essential component of SNNs is the spiking neuron, which encodes information with binary spikes over several time steps, thus avoiding multiplication during inference. In recent years, with the development of novel training algorithms, SNNs have achieved competi-  
10 tive performance on several tasks, such as image classification (Meng et al., 2022), object detection (Kim et al., 2020), and object segmentation (Patel et al., 2021). Meanwhile, the development of neuromorphic hardware further improves the performance of SNNs. For instance, the recently released second-generation neuromorphic research chip Loihi 2 (Orchard et al., 2021)

15 supports larger neural architectures and new applications while providing faster and energy-efficient processing.

However, the development of SNN architectures is lagging behind. Unlike ANN, SNN has a two-dimensional computational graph containing both spatial and temporal domains. Most previous studies simply utilize ANN architectures like VGG-Net (Simonyan and Zisserman, 2015), and ResNet (He et al., 2016), ignoring the architecture gap between ANNs and SNNs. On the other hand, directly applying typical neural architecture search (NAS) methods such as ENAS (Pham et al., 2018) and DARTS (Liu et al., 2019) on searching SNN architectures can be very time-consuming due to the much slower training speed of SNNs. Existing NAS methods for SNNs (Kim et al., 2022; Na et al., 2022; Che et al., 2022) manage to accelerate the training process by imposing limitations on the search space. For instance, SNASNet (Kim et al., 2022) is selected from a cell-based search space with only four nodes in each cell. SpikeDHS (Che et al., 2022) adopts a hierarchical search space also with four nodes in each cell. AutoSNN (Na et al., 2022) searches the hyperparameters of each spiking block under a pre-defined macro architecture. We note that these works do not pay enough attention to the connection topology of the SNN architecture. Their search space highly restricts the connection topology of the SNN structure, which may cause a severe loss of architecture diversity, resulting in missing the optimal SNN architecture. Therefore, it is necessary to design a dedicated search space for SNN architectures, which has a higher degree of freedom on the connection topology design.

In this study, we aim to exploit the potential of the topology design on

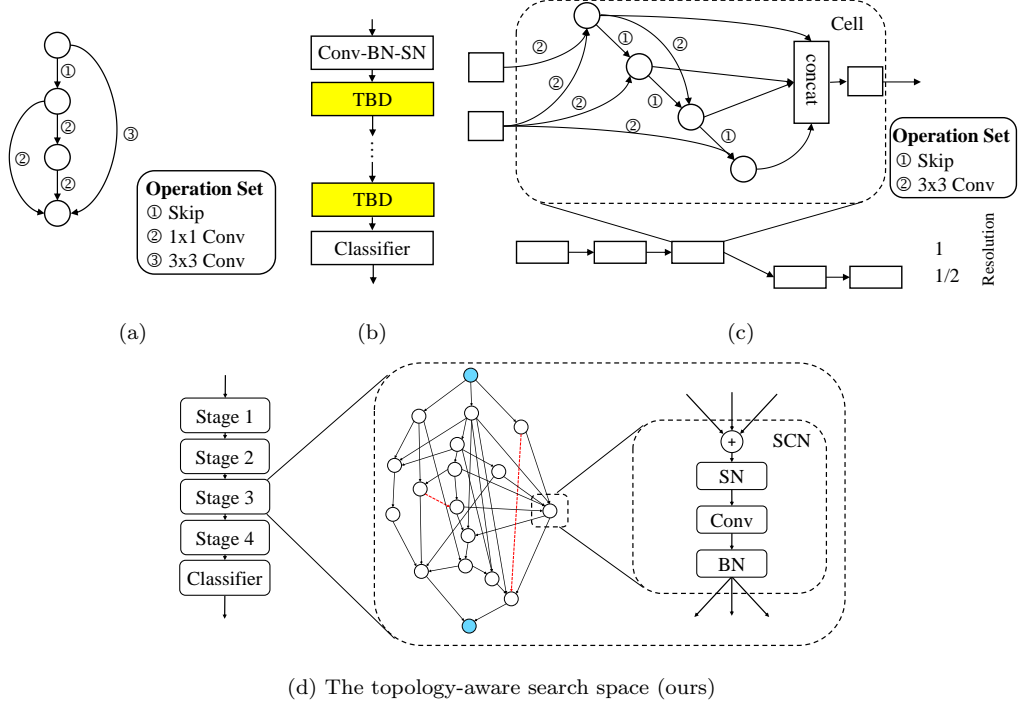


Figure 1: A comparison of different search space designs for SNNs. (a) SNASNet (Kim et al., 2022) adopts a cell-based search space. The cell has a total of four nodes, and each edge is associated with an operation selected from the operation set. (b) AutoSNN (Na et al., 2022) employs a fixed topology while searching for the optimal choices for the to-be-determined (TBD) blocks. (c) SpikeDHS (Che et al., 2022) utilizes a search space similar to DARTS (Liu et al., 2019), with 4 nodes within a cell, and extends its search to the layer level. (d) We present the topology-aware search space enabling complex designs of spatial and temporal topologies. Our architecture comprises multiple stages, each represented by a connection topology graph. In this illustration, Stage 3 consists of 16 spiking convolution nodes (SCNs) in white, along with a source node and a sink node, both colored blue. Each SCN transforms the summation of the input data through a layer of spiking neurons (SN), a convolutional layer, and a batch normalization layer (BN). Directed connections between nodes are indicated by arrows, while red dashed arrows represent connections with synaptic delay.

40 both spatial and temporal dimensions for SNNs. To this end, we propose  
 the topology-aware search space specifically for searching SNN architectures,  
 which enables a more complex connection topology of the network. The  
 topology-aware search space has a larger topology graph with at most 32  
 nodes, which is **eight times larger** than that in previous studies (Kim  
 45 et al., 2022; Che et al., 2022). We also incorporate the synaptic delay within  
 our architecture, thereby enabling the design of the temporal topology. This  
 provides a novel perspective to better leverage the temporal processing ability  
 of SNN by the architecture design. Fig. 1 illustrates the difference between  
 our work and previous studies. Note that there is a huge number of possible  
 50 connection topologies in the topology-aware search space. Learning to search  
 for architectures in such an ample search space is a big challenge, *especially*  
*due to the high training cost* of SNN architectures (Kim et al., 2022; Wu  
 et al., 2018). Nevertheless, we notice that random algorithms (Sciuto et al.,  
 2020; Xie et al., 2019; Li and Talwalkar, 2019) can also yield competitive  
 55 performance compared with other NAS methods. Inspired by these works,  
 we propose the spatio-temporal topology sampling (STTS) algorithm to ob-  
 tain SNN architectures efficiently. In the proposed algorithm, we use random  
 graph models to generate the spatial topology and sample the synaptic de-  
 lay from a pre-defined distribution to generate the temporal topology. *By*  
 60 *leveraging the efficiency of random sampling, STTS avoids the search process*  
*and can obtain a powerful architecture **within 0.1 seconds**, representing*  
*a significant acceleration compared with existing NAS methods on SNNs.*  
 We evaluate our method on CIFAR-10 (Krizhevsky et al., 2009), CIFAR-100  
 (Krizhevsky et al., 2009) and ImageNet (Deng et al., 2009) datasets. Our

65 method achieves state-of-the-art accuracy on nearly all datasets, while having a lower energy consumption compared with prior works. We summarize our contributions as follows:

1. We propose the topology-aware search space explicitly designed for SNN architecture searching. With the topology-aware search space, it  
70 is the first time that we can introduce much more diverse connection topologies into the design of SNN architectures.
2. We propose to consider the synaptic delay in the topology-aware search space, which enables a more flexible design of the temporal topology. This presents a novel perspective for exploiting the temporal learning  
75 capacity of SNNs by the architecture design.
3. We propose the spatio-temporal topology sampling (STTS) algorithm to sample architectures from our search space. Our algorithm provides an alternative way to obtain SNN architectures, avoiding the huge searching cost in previous studies.

## 80 2. Related Works

There are mainly two strategies to obtain an SNN architecture: leveraging ANN architectures, and applying the NAS methods to search for SNN architectures directly.

### *2.1. Leveraging ANN Architectures*

85 Converting ANNs to SNNs (Rueckauer et al., 2017; Kugele et al., 2020) is one of the most effective methods for training SNNs. This approach leverages ANN architectures inherently. Consequently, a majority of subsequent

SNN studies (Han et al., 2020; Rathi et al., 2020; Zheng et al., 2021; Meng et al., 2022; Deng et al., 2022; Bu et al., 2022) also make use of ANN architectures. Typical ANN architectures, such as VGG-Net (Simonyan and Zisserman, 2015), and ResNet (He et al., 2016), can be adapted to SNNs by replacing the ReLU activation function with spiking neurons. Based on the ANN backbone, some SNN-friendly modifications have been proposed, such as tDBN (Zheng et al., 2021), PLIF neuron (Fang et al., 2021b), and SEW block (Fang et al., 2021a). However, naively leveraging ANN architectures is not optimal due to the inherent architectural gap between ANNs and SNNs (Kim et al., 2022).

## 2.2. Neural Architecture Search

Neural architecture search (NAS) methods are proposed for searching optimal neural architectures in an automated way. Early NAS method (Zoph and Le, 2017) defines a global search space and uses reinforcement learning (RL) as the search strategy. To search neural architectures more effectively and efficiently, recent studies in the field of NAS focus on optimization strategies, including modular search space (Zoph et al., 2018), continuous search strategy (Liu et al., 2019; Wu et al., 2019; Dong and Yang, 2019), weight-sharing strategy (Pham et al., 2018; Cai et al., 2019; Bender et al., 2018; Na et al., 2022; Guo et al., 2020), and random algorithms (Xie et al., 2019; Li and Talwalkar, 2019; Sciuto et al., 2020). However, these methods are for searching ANN architectures only.

Recently, NAS methods have been utilized to obtain SNN architectures directly, but the related work is very limited. Kim et al. (2022) are the first to apply a NAS method for searching SNN architectures. They evaluate the



representation power of each candidate architecture at initialization, thereby avoiding the training cost. Na et al. (2022) investigate design choices concerning both accuracy and number of spikes. They introduce a spike-aware evolutionary algorithm, aiming to discover an SNN architecture that achieves high accuracy and generates fewer spikes. Che et al. (2022) present a differentiable hierarchical search framework that encompasses both cell-level and layer-level search spaces. Additionally, they extend their approach to include surrogate gradient search. However, the search space in these methods is quite small, which highly restricts the topology design of the SNN architecture. In contrast, we propose to introduce a much more complex connection topology into the design of SNN architectures.

### 3. Preliminary

#### 3.1. The Leaky Integrate-and-Fire (LIF) Model

The fundamental component in SNNs to process binary information is the spiking neuron. Similar to previous SNN studies (Fang et al., 2021a; Kim et al., 2022; Na et al., 2022), we adopt the discrete version of the Leaky Integrate-and-Fire (LIF) model to describe the spatio-temporal dynamics of the spiking neuron, which can be formulated as

$$H^l[t] = V^l[t - 1] + \frac{1}{\tau}(X^l[t] - (V^l[t - 1] - V_{reset})), \quad (1)$$

$$S^l[t] = \Theta(H^l[t] - V_{th}), \quad (2)$$

$$V^l[t] = H^l[t](1 - S^l[t]) + V_{reset}S^l[t], \quad (3)$$

where  $l$  is the layer index,  $\tau$  is the membrane time constant,  $X[t]$  is the input current at time step  $t$ ,  $H[t]$  represents the membrane potential before the

trigger of a spike, and  $V[t]$  denotes the membrane potential after triggering.  $\Theta(x)$  is the Heaviside step function. A spike is triggered if  $H[t]$  exceeds the firing threshold  $V_{th}$ . We use hard reset here, which means that the spiking neuron resets its membrane potential to  $V_{reset}$  after firing a spike.

### 3.2. Spatio-temporal Backpropagation

Due to the non-differentiability of the spike function, the training of SNN is a great challenge. Recent works on directly training SNN (Fang et al., 2021a; Deng et al., 2022) adopt the spatio-temporal backpropagation (STBP) training framework (Wu et al., 2018). These works regard the SNN as a recurrent neural network (RNN) and calculate the gradient by the backpropagation on both spatial and temporal dimensions. We use the same method, which is formulated as

$$\frac{\partial \mathcal{L}}{\partial \mathbf{W}} = \sum_{t=1}^T \frac{\partial \mathcal{L}}{\partial H^l[t]} \frac{\partial H^l[t]}{\partial X^l[t]} \frac{\partial X^l[t]}{\partial \mathbf{W}}, \quad (4)$$

where  $\mathcal{L}$  denotes the loss function,  $T$  is the number of time steps. Since the Heaviside step function is non-differentiable, previous studies (Wu et al., 2018; Fang et al., 2021a; Deng et al., 2022) approximate its gradient with some surrogate gradients. [Following these studies, we employ the same surrogate gradient as utilized in some previous works \(Fang et al., 2021a,b\):](#)

$$\frac{\partial S^l[t]}{\partial H^l[t]} = \frac{\alpha}{2 \left[ 1 + \left( \frac{\pi}{2} \alpha H^l[t] \right)^2 \right]}, \quad (5)$$

where  $\alpha$  denotes the slope parameter.

## 4. Methodology

### 4.1. Topology-aware Search Space

The cell-based search space has been widely used in modern NAS algorithms (Liu et al., 2019; Zoph et al., 2018; Dong and Yang, 2020). In the cell-based search space, the final architecture is constructed from a few types of small cell structures, thereby significantly reducing the search complexity. However, the cell-based search space is not suitable for searching SNN architectures mainly because it highly restricts the design of the spatial topology as well as the temporal topology of the SNN architecture. Thus, designing a search space explicitly for SNN architectures is important. To this end, we propose the topology-aware search space, an SNN-friendly search space focusing on increasing the diversity of both spatial and temporal connection topologies.

As shown in Fig. 1d, each stage in our search space can be represented by a connection topology graph. The connection topology graph consists of several spiking convolution nodes and some edges connecting the nodes. Unlike conventional representations associating operations with edges (Dong and Yang, 2020), we define operations inside each spiking convolution node, and an edge represents information transmission between a pair of nodes.

**Spiking convolution node.** The spiking convolution node (SCN) is the basic computing unit in the topology-aware search space. As shown in Fig. 1d, SCN has some input edges as well as output edges. The node first receives input data from all the input edges, then aggregates all the input data via a simple summation. Afterwards, the aggregated data are transformed sequentially through a layer of spiking neurons (SN), a convolutional layer, and a

batch normalization layer (BN). Finally, the node sends out the transformed data through its output edges. We can formulate the node operations as

$$X_j[t] = \sum_{(i,j) \in E} S_i[t], \quad (6)$$

$$S_j[t] = \text{BN}(\text{Conv2d}(\text{SN}(X_j[t]))), \quad (7)$$

where  $X_j[t]$  and  $S_j[t]$  represent the aggregated data and transformed data of the  $j$ -th node at time step  $t$ , respectively. In the topology-aware search space, we do not search for the choice of operations. We adopt the SN-convolution-BN triplet inside all spiking convolution nodes. During the inference, we will merge the BN layer into the precedent convolutional layer.

**Spatial connection topology.** In our topology-aware search space, the spatial connection topology can be represented as a directed acyclic graph (DAG)  $G = (V, E)$ . For simplicity, we assume that nodes in the DAG are sorted in a topology order. An edge only points to the node with a higher index from the node with a smaller index. Benefiting from these settings, we have a high degree of freedom to design the spatial connection topology, especially when the number of nodes is large (*e.g.*  $|V| = 16, 32$ ). For instance, considering a DAG with  $|V|$  nodes, there are  $2^{\frac{|V|(|V|-1)}{2}}$  different graphs if ignoring the isomorphism of graphs.

**Temporal connection topology.** Due to the spatio-temporal dynamics of the spiking neuron, SNN has not only spatial connection topology, but also temporal connection topology. The temporal connection topology of SNN, controlled by the synaptic delay, has an important impact on the effectiveness and efficiency of SNN (Maass, 1997). However, most existing works ignore the synaptic delay, restricting the utilization of temporal information. We

propose to incorporate the synaptic delay into our topology-aware search space to enable temporal topology design. In our topology-aware search space, each edge is assigned an extra parameter, controlling the synaptic delay on the edge. We adopt a simplified modeling of synaptic delay in which synaptic delay is restricted to discrete values. In this model, the operations inside SCN in Eq. (6) are modified as

$$X_j[t] = \sum_{(i,j) \in E} S_i[t - d_{(i,j)}], \quad (8)$$

where  $d_{(i,j)}$  is a nonnegative integer, representing the discrete synaptic delay associated with edge  $(i, j)$ . The output data sent out from the  $i$ -th node at time step  $t - d_{(i,j)}$  arrives at the  $j$ -th node at time step  $t$  through edge  $(i, j)$  after a synaptic delay of  $d_{(i,j)}$ . When  $t$  is smaller than  $d_{(i,j)}$ , we assume that  $S_i[t - d_{(i,j)}]$  is a zero tensor. Additionally,  $d_{(i,j)} = 0$  is possible in this model, which means that there is no synaptic delay on edge  $(i, j)$ , and the operations are simplified as in Eq. (6).

**Source and sink.** We have defined the spiking convolution node and the connection topology graph. Besides, we need to specify the input and the output of the whole graph in order to convert the connection topology graph into a valid neural network. Note that there are still some nodes that do not have any input edge or output edge. For the nodes without any input edge, we define them as input nodes. Similarly, nodes without any output edge are defined as output nodes. We use  $\mathcal{S}$  to denote the set of input nodes and  $\mathcal{T}$  to represent the set of output nodes. A common approach to deal with multiple input and output nodes is to create a unique source node connecting to all the input nodes and a unique sink node receiving outputs from all the

output nodes, as shown in Fig. 1d. Specifically, we assume that the source node sends a copy of input data to every input node while the sink node collects a mean from all the output nodes. We can formulate it as

$$X_j[t] = \begin{cases} X[t], & \text{if } j \in \mathcal{S}, \\ \sum_{(i,j) \in E} S_i[t - d_{(i,j)}], & \text{otherwise,} \end{cases} \quad (9)$$

and

$$S[t] = \frac{1}{|\mathcal{T}|} \sum_{i \in \mathcal{T}} S_i[t], \quad (10)$$

225 where  $X[t]$  and  $S[t]$  denote the input and the output of the whole graph at time step  $t$ , respectively. Note that the output of the whole graph is a summation of  $|\mathcal{T}|$  tensors, then be divided by  $|\mathcal{T}|$ . Since  $|\mathcal{T}|$  is fixed as soon as the graph is determined, the division operation can be replaced by scaling up the firing threshold by  $|\mathcal{T}|$  in the following spiking neurons.

230 **Stages.** It is very common (Simonyan and Zisserman, 2015; He et al., 2016; Xie et al., 2019) for neural architectures to have multiple stages to down-sample the feature maps from high resolution to low resolution, especially for image classification and object detection. Inspired by these works, We divide our entire model into several stages that generate different sizes of feature maps. Each stage is defined by a connection topology graph described above. For two adjacent stages, the preceding stage’s sink node is also the succeeding stage’s source node.

Regarding image input, we assume that the input resolution for the  $i$ -th stage is  $H_i \times W_i$  with  $C_i$  channels. To make a  $2 \times$  downsampling of the resolution, we use a stride of 2 and an output channel number of  $2C_i$  in

240

the convolutional layer inside each input node. For other nodes in the same stage, a stride of 1 is used, and the input and the output channel numbers are both  $2C_i$ . By doing so, the output of the  $i$ -th stage has a dimension of  $2C_i$  with a resolution of  $\frac{H_i}{2} \times \frac{W_i}{2}$ .

245 The class of architectures defined by the topology-aware search space is named the topology-aware network (TANet). We adopt a similar macro skeleton as previous studies (Xie et al., 2019). Table 1 summarizes two settings of our TANet: the tiny version, referred to as TANet-Tiny, and the regular version, referred to as TANet-Regular. The TANet-Tiny has four  
250 stages in total. It is designed for datasets with a smaller resolution, such as CIFAR-10 and CIFAR-100. The TANet-Regular has five stages and is proposed for larger resolution datasets such as ImageNet. Both TANet-Tiny and TANet-Regular have a classifier in the end.

#### 4.2. Spatio-temporal Topology Sampling

255 Modern NAS methods (Liu et al., 2019; Pham et al., 2018) have already achieved state-of-the-art performance on many tasks. However, these methods are not suitable for searching SNN architectures from the topology-aware search space, due to the huge number of candidate architectures in the search space and the high training cost of directly training SNNs (Kim et al., 2022).  
260 Nevertheless, recent works on random sampling (Xie et al., 2019; Sciuto et al., 2020) have given us an alternative approach to yield powerful neural architectures without high searching costs. In these works, neural architectures are sampled from the search space through some pre-defined random algorithms. Inspired by these studies, we propose the spatio-temporal topology  
265 sampling (STTS) algorithm to sample SNN architectures from the topology-

Stage	TANet-Tiny	TANet-Regular
1	single node $C$	single node $C/2$
2	single node $C$	graph $N/2, C$
3	graph $N, 2C$	graph $N, 2C$
4	graph $N, 4C$	graph $N, 4C$
5	-	graph $N, 8C$
	classifier	

Table 1: Two settings of TANet. Each stage is generated from a connection topology graph. For each graph,  $N$  denotes the number of nodes, and  $C$  represents the output channel. We set  $N = 1$  for the first few stages, where the graph becomes a single node.



aware search space randomly. Different from random search algorithm (Li and Talwalkar, 2019), STTS does not evaluate the performance of candidate architectures but directly outputs the sampled architecture as the final architecture. Therefore, STTS is very efficient compared with other NAS  
 270 methods.

Specifically, in STTS, we sample the spatial topology as well as the temporal topology for each stage. As shown in Algorithm 1, STTS consists of two procedures: 1) using random graph models to generate the spatial topology and 2) sampling the synaptic delay of each edge from a pre-defined  
 275 distribution to generate the temporal topology. As soon as we determine the connection topology graph, we convert the graph into a valid neural network. Finally, we stack stages sequentially and output the final architecture.

In practice, we use the Watts-Strogatz (WS) model (Watts and Strogatz, 1998) and the Barabási-Albert (BA) model (Albert and Barabási, 2002) to  
 280 generate the spatial topology in the first procedure. We describe the details in Appendix A. Since the random graph models generate undirected graphs, we have to convert the undirected graph to a DAG. To do so, we randomly assign a topology order. Then each edge is directed from the node with a smaller index to the node with a higher index. In the second procedure, we  
 285 randomly sample the synaptic delay of each edge independently from a pre-defined distribution  $\mathcal{D}_{sd}$ . We set the synaptic delay to be either 0 or 1, and  $\mathcal{D}_{sd}$  is a Bernoulli distribution. The parameter  $p$  in the Bernoulli distribution is referred to as the synaptic delay parameter, which controls the temporal connection topology.

290 Although STTS directly outputs the final architecture without evalua-

tion, as we will see in the experimental results section, sampling multiple architectures leads to similar accuracies after training.

---

**Algorithm 1:** Spatio-temporal topology sampling

---

**Input:** Random graph model; Number of stages  $n$ ; Synaptic delay

distribution  $\mathcal{D}_{sd}$ ;

**for**  $i = 1$  *to*  $n$  **do**

    Generate spatial topology  $G_i = (V_i, E_i)$  through the random graph model;

**foreach**  $e$  *in*  $E_i$  **do**

        | Sample the synaptic delay of edge  $e$  from  $\mathcal{D}_{sd}$ ;

**end**

    Covert the connection topology graph into a valid neural network;

**end**

Stack each stage sequentially to construct the final architecture.

---

## 5. Experiments

We conduct extensive experiments to verify the effectiveness of our proposed method. The implementation details of these experiments are described in Appendix B.

### 5.1. Architecture Details

We use two settings of TANet in our experiments: TANet-Tiny for CIFAR-10/100 and TANet-Regular for ImageNet. We set the number of nodes  $N$  to 32 and the number of channels  $C$  to 96 for both TANet-Tiny and TANet-Regular. For the synaptic delay parameter  $p$ , we set it to 0.05 for both

TANet-Tiny and TANet-Regular. We use the BA graph model and the WS graph model to generate the spatial topology of TANet-Tiny and TANet-Regular, respectively. Between the final stage and the classifier, there is a layer of spiking neurons. The classifier consists of a  $1 \times 1$  convolution-BN-SN triplet, a global average pooling layer, and a voting layer. To avoid overfitting, We add a dropout (Srivastava et al., 2014) layer between the average pooling layer and the voting layer in the classifier of TANet-Tiny, and we set the drop probability to 0.2.

We use depthwise separable convolution (Chollet, 2017) in every spiking convolution node. The depthwise separable convolution consists of two layers: the depthwise convolution and the pointwise convolution. The depthwise convolution has a kernel size of  $3 \times 3$  while the pointwise convolution has a kernel size of  $1 \times 1$ . Note that we can transform the depthwise separable convolution into a standard convolution with the same function. Therefore, we use depthwise separable convolutions in the training process and replace them with equivalent convolutions during the inference.

## 5.2. Similarity between Different Samples

In the STTS algorithm, we sample architecture once without evaluation. This raises the question of whether different samples will exhibit significant variation in accuracy after the training process. In this section, we empirically demonstrate the similarities between different samples and show that sampling multiple architectures leads to similar accuracies after training.

It is noteworthy that the architectures we sampled with different seeds all utilize the same graph model for generating spatial topology and the same distribution for generating temporal topology. Consequently, these samples

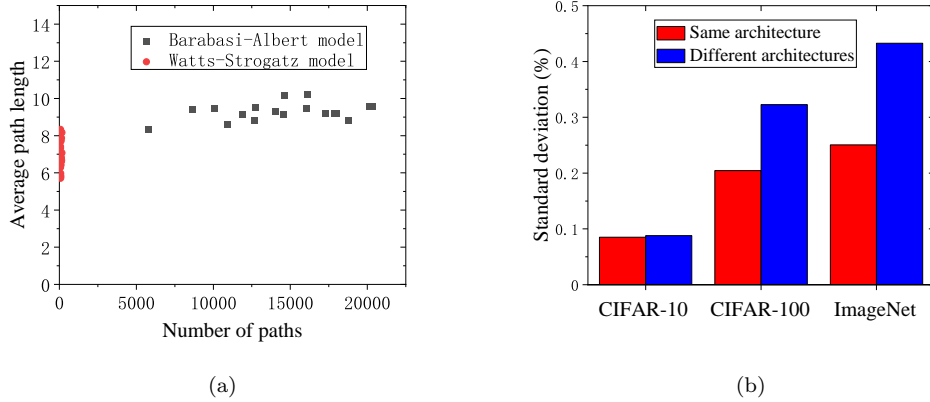


Figure 2: Similarity between different samples. (a) The number of paths and the average path length across different samples. (b) The standard deviation across several training runs of the same architecture and across different samples.

inherently exhibit similarities. To quantify these similarities, we calculate two important statistical values of the spatial topology across these samples: the number of paths and the average path length. The results are presented in Fig. 2a. Notably, instances sampled from the same graph model exhibit clear similarities. Specifically, instances sampled from the WS model demonstrate similar numbers of paths, while those sampled from the BA model exhibit comparable average path lengths.

Additionally, we calculate the standard deviation across multiple training runs of the same architecture and compare it to the standard deviation across different samples. The results are shown in Fig. 2b. Notably, the variation across different samples is slightly larger than that observed across several training runs of the same architecture. However, it’s important to highlight that in both cases, the standard deviation remains relatively low.

	Method	Architecture	Params	Time steps	Accuracy (%)
CIFAR-10	Rathi et al. (2020)	VGG-9	32M	100	90.54
	Yan et al. (2021)	VGG-like	9M	600	94.16
	Zheng et al. (2021)	ResNet-19	13M	6	93.16
	Deng et al. (2022)	ResNet-19	13M	4	94.44
	Kim et al. (2022)	Searched Architecture	20M	5	92.73
	Na et al. (2022)	Searched Architecture	21M	8	93.15
	Che et al. (2022)	Searched Architecture	14M	6	<b>95.50</b>
	STTS (ours)	TANet-Tiny	7M	4	95.10 $\pm$ 0.09
CIFAR-100	Rathi et al. (2020)	VGG-11	37M	125	67.87
	Yan et al. (2021)	VGG-like	9M	300	71.84
	Deng et al. (2022)	ResNet-19	13M	4	74.47
	Kim et al. (2022)	Searched Architecture	21M	5	73.04
	Na et al. (2022)	Searched Architecture	5M	8	69.16
	Che et al. (2022)	Searched Architecture	14M	6	76.25
	STTS (ours)	TANet-Tiny	7M	4	<b>76.33<math>\pm</math>0.32</b>
ImageNet	Rathi et al. (2020)	VGG-16	138M	250	65.19
	Rathi and Roy (2021)	VGG-16	138M	5	69.00
	Fang et al. (2021a)	SEW-ResNet-50	26M	4	67.78
	Deng et al. (2022)	SEW-ResNet-34	22M	4	68.00
	Che et al. (2022)	Searched Architecture	58M	6	68.64
	STTS (ours)	TANet-Regular	25M	4	<b>70.79<math>\pm</math>0.43</b>

Table 2: Comparison between our work and other methods on CIFAR-10, CIFAR-100, and ImageNet. “Params” denotes the number of parameters in the architecture. [We report the mean and standard deviation accuracy \(after  \$\pm\$ \) of five runs under different random seeds.](#)

### 340 5.3. Comparison to the State of the Art

We compare our experimental results with some SOTA methods on CIFAR-10, CIFAR-100, and ImageNet. The results are summarized in Table 2.

For the CIFAR-10 dataset, our architecture achieves competitive accuracy among all other methods. The reported mean accuracy of TANet-Tiny is  
345 only 0.4% lower than the SpikeDHS (Che et al., 2022), although TANet-Tiny uses a much less number of parameters and time steps. The results also show that the variation of the corresponding accuracies among the sampled architectures is low. The classification accuracy only has a standard deviation of 0.09% among these samples.

350 We can see that our method has a significant improvement on more difficult datasets. For the CIFAR-100 dataset, our architecture yields state-of-the-art results using only 4 time steps. Specifically, TANet-Tiny achieves a mean accuracy of 76.33%, which performs 0.08% advance compared to SpikeDHS. It is noteworthy that although we only focus on designing SNN  
355 architectures, our method outperforms these works that include both training methods and architecture designs.

For the ImageNet dataset, our architecture has 70.79% top-1 accuracy using 4 time steps, achieving a 3.01% increment compared with SEW-ResNet-50 and a 2.15% increment compared with SpikeDHS. Note that our architec-  
360 ture has fewer parameters and uses a similar or much less number of time steps.

### 5.4. Analysis on the Topology-aware Search Space

We conduct experiments to validate the suitability of our topology-aware search space for obtaining SNN architectures. In our comparison, we evaluate

Architecture	w/o SN (%)	w/ SN (%)
SEW-ResNet-50	76.34 $\pm$ 0.12	66.16 $\pm$ 0.11
TANet-Regular (ours)	74.93 $\pm$ 0.27	70.79 $\pm$ 0.43

Table 3: Comparison with SEW-ResNet backbone on ImageNet. “w/o SN” and “w/ SN” represent the SNN architecture and the ANN architecture using the same backbone, respectively. We report the mean and standard deviation accuracy (after  $\pm$ ) of five runs under different random seeds.

Number of nodes	8	16	32	48	64
Accuracy (%)	94.81 $\pm$ 0.07	94.93 $\pm$ 0.07	94.99 $\pm$ 0.04	94.58 $\pm$ 0.12	94.27 $\pm$ 0.11

Table 4: Effect of the size of the graph on CIFAR-10. We report the mean and standard deviation accuracy (after  $\pm$ ) of three runs under different random seeds.

365 TANet-Regular alongside SEW-ResNet-50 (Fang et al., 2021a), which is an  
SNN-friendly modification of the conventional ANN architecture ResNet (He  
et al., 2016). To ensure a fair comparison, we use identical hyperparameters  
and training methods for both models. The results are shown in Table 3.  
Under the same training settings, TANet-Regular achieves a 4.63% higher  
370 classification accuracy compared to SEW-ResNet-50 in the context of SNNs.  
These experimental results strongly demonstrate that typical ANN architec-  
tures are not optimal for SNNs. Our topology-aware search space proves to  
be an SNN-friendly search space that can further exploit the potential of  
SNN structures.

### 375 5.5. Effect of the Size of the Graph

We test the effect of the size of the graph in the topology-aware search space. In details, We vary the number of nodes in the graph from 8 to 64 while adjusting the number of channels to keep the total number of parameters. The results are shown in Table 4. We can see that as we increase the  
380 number of nodes from 8 to 32, the performance improves, implying that SNN architectures benefit from a more complex connection topology. However, as the number of nodes continuing increasing from 32 to 64, the accuracy becomes lower and lower. This might be because the decreasing of the number of channels has a more significant impact as we increase the number of nodes.  
385 Additionally, increasing the number of nodes might lead to overfitting.

### 5.6. Effect of the Synaptic Delay

We conduct experiments to analyze the influence of the synaptic delay parameter  $p$ . We vary  $p$  from 0 to 0.2, where  $p = 0$  means no synaptic delay in the architecture. The results are shown in Fig. 3. We can see that the  
390 architecture is not optimal when there is no synaptic delay. When we increase  $p$  to 0.05, we observe a slight improvement in classification accuracies for CIFAR-100 and ImageNet. However, as we continue increasing the synaptic delay parameter  $p$  (e.g.  $p = 0.15, 0.2$ ), the accuracy begins to decrease. We choose  $p = 0.05$  for optimal on all the datasets.

### 395 5.7. Energy Efficiency

In contrast to ANNs, SNNs perform event-based operation and multiplication-free inference. In this section, we demonstrate the energy efficiency of our method by measuring the sparsity and energy consumption of TANet.



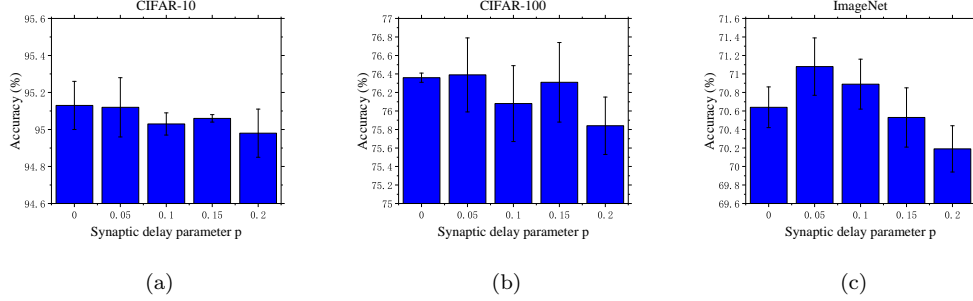


Figure 3: Effects of the synaptic delay parameter  $p$  on (a) CIFAR-10, (b) CIFAR-100, and (c) ImageNet.

**Sparsity.** To provide a comprehensive insight into the sparsity of our architecture, We calculate both the average firing rate (per time step) and the spike count for each SCN in our architecture. Fig. 4 visualizes the sparsity statistics at different stages. The experimental results reveal a notably sparse spiking activity within our architecture. Specifically, concerning firing rates, the majority of nodes exhibit average firing rates of less than 10% in TANet-Tiny and less than 15% in TANet-Regular. In terms of spike counts, the majority of nodes generate fewer than 30K spikes in TANet-Tiny and 500K spikes in TANet-Regular. Both of these two sparsity statistics exhibit distinct patterns at different stages, with the firing rate and spike count decreasing as the neural network’s depth increases.

**Energy consumption.** Following previous studies (Li et al., 2021; Deng et al., 2022; Che et al., 2022), we estimate the energy consumption of our architecture by measuring the number of synaptic operations. For more details of the energy consumption analysis, please refer to Appendix C. We conduct a comprehensive analysis of energy consumption, comparing our architectures with typical ANN architecture, SNN architecture searched by

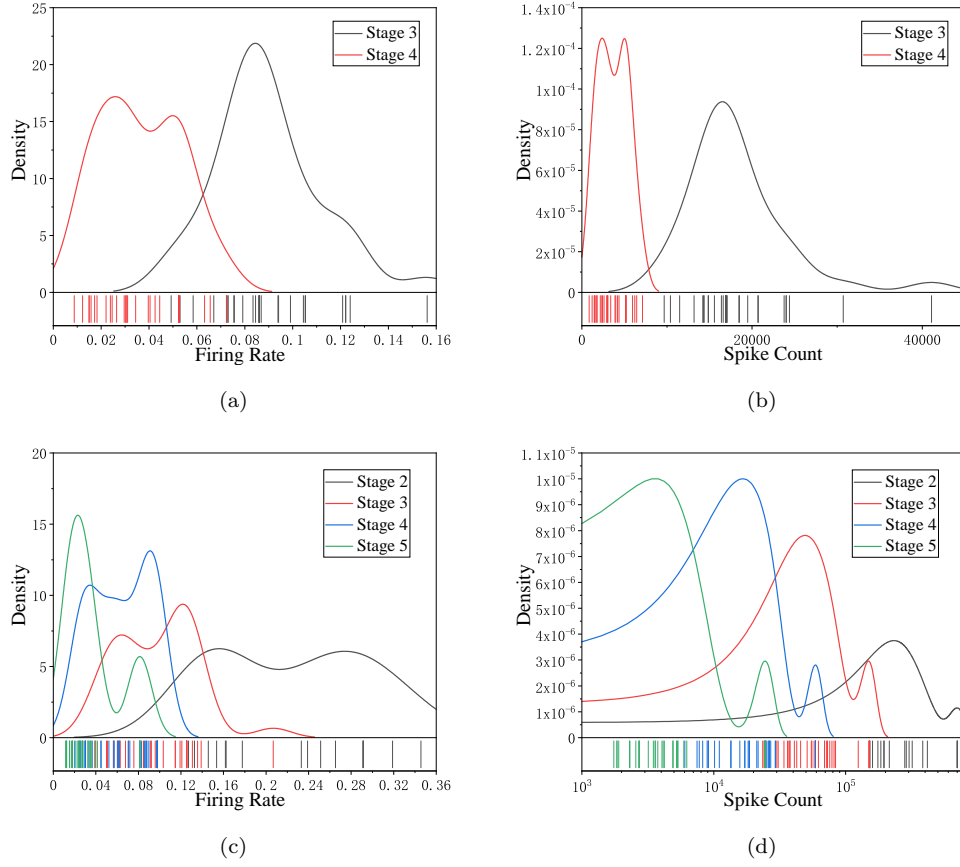


Figure 4: Sparsity statistics at different stages. (a) Firing rate distribution in TANet-Tiny. (b) Spike count distribution in TANet-Tiny. (c) Firing rate distribution in TANet-Regular. (d) Spike count distribution in TANet-Regular.

	Architecture	#Add.	#Mult.	Energy (mJ)
CIFAR-10	ResNet-19 (ANN)	2285M	2285M	10.5
	TANet-Tiny (ANN)	735M	735M	3.4
	SpikeDHS (SNN)	5973M	19M	5.5
	TANet-Tiny (ours)	1329M	3M	<b>1.2</b>
ImageNet	ResNet-50 (ANN)	4134M	4134M	19.0
	TANet-Regular (ANN)	3093M	3093M	14.2
	TANet-Regular (ours)	9026M	16M	<b>8.2</b>

Table 5: The operation number and energy consumption. “# Add.” and “#Mult.” represent the number of addition and multiplication operations, respectively.

SpikeDHS (Che et al., 2022), and ANN versions of our architectures. The results are shown in Table 5. We can see that our architectures achieve the lowest energy consumption among these architectures.

## 6. Conclusion and Future Work

420 In this paper, we propose the topology-aware search space to expand the range of design choices for SNN architectures. The topology-aware search space not only enables complex designs of spatial topology but also empowers the design of temporal topology by incorporating the synaptic delay. Instead of utilizing a classical NAS method, we propose the spatio-temporal topology  
425 sampling (STTS) algorithm to obtain SNN architectures from our search space. By avoiding the unaffordable NAS cost, our algorithm is much more efficient compared with previous studies. Experimental results show that

our proposed method achieves state-of-the-art accuracy and generates fewer spikes on image classification tasks. Our method highlights the significance  
430 of the connection topology in designing SNN architectures.

For our work, there is still a lack of theoretical guarantee of the random sampling method, although empirical results show that the variance between different sampled architectures is low. In future research, we plan to analyze the effectiveness of different topologies in SNNs theoretically. We will  
435 also investigate the correlation between the spatial topology and the temporal topology. We aim to propose a robust NAS method with a theoretical guarantee and yield more powerful SNN architectures.

## Acknowledgements

Z. Lin was supported by National Key R&D Program of China (2022ZD0160302),  
440 the NSF China (No. 62276004), the major key project of PCL, China (No. PCL2021A12), and Qualcomm.

## Appendix A. Random Graph Models

To generate network topologies, Xie et al. (2019) use random graph models from graph theory. Inspired by their works, we use the the Watts-Strogatz  
445 (WS) model (Watts and Strogatz, 1998) and the Barabási-Albert (BA) model (Albert and Barabási, 2002) to generate the spatial topology. We describe them in the following.

**Watts-Strogatz.** The WS model is a random graph model which can generate graphs with small-world properties. To generate an undirected graph  
450 with  $N$  nodes, the WS model contains two procedures: 1) Place the  $N$  nodes

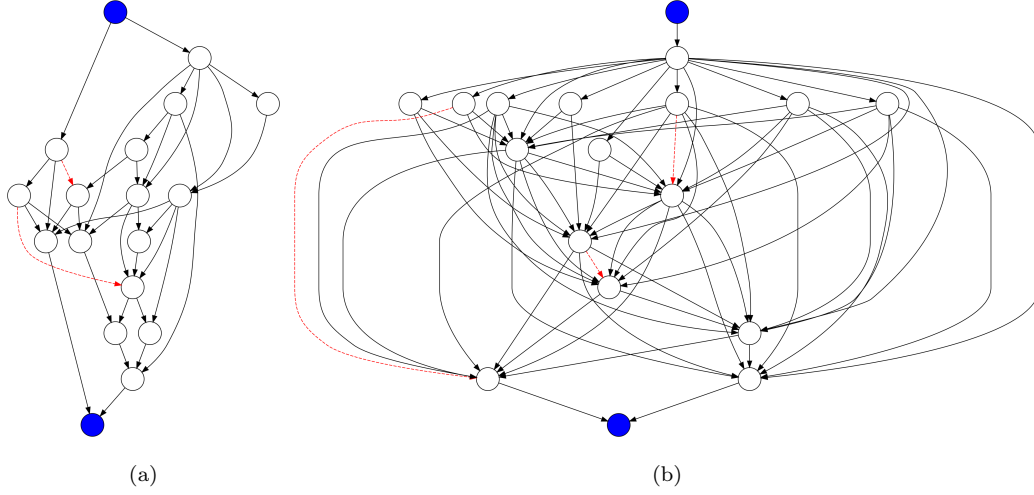


Figure A.5: Two topology graph instances. (a) A topology graph with the spatial topology generated by the WS model. (b) A topology graph with the spatial topology generated by the BA model. Nodes representing the source and sink are highlighted in blue, while red dashed arrows represent connections with synaptic delays.

in a regular ring lattice. Each node is connected to  $K$  neighbors, with  $K/2$  on both sides. 2) For every node  $v$ , the edge that connects  $v$  to its  $K/2$  rightmost neighbors is rewired with probability  $P$ . “Rewire” means that the edge is replaced with edge  $(v, k)$  where the node  $k$  is uniformly chosen at  
455 random while avoiding duplication.

**Barabási-Albert.** The BA model is a random graph model which generates scale-free networks. The graph begins with  $M$  nodes without any edges. Then, new nodes are sequentially added to the graph, one at a time. Each new node will be connected to  $M$  existing nodes with a probability proportional to the degrees of the existing nodes.  
460

In our experiments, we set  $K = 4, P = 0.75$  for the WS model and  $M = 8$  for the BA model. Consequently, in the case of TANet-Tiny, a graph

with 32 nodes exhibits dense connectivity, with a total of 192 edges. In the configuration of TANet-Regular, a 32-node graph has 64 edges, representing a sparser connectivity pattern. We visualize two examples in Fig. A.5.

## Appendix B. Implementation Details

### *Appendix B.1. Datasets*

We conduct experiments on CIFAR-10 (Krizhevsky et al., 2009), CIFAR-100 (Krizhevsky et al., 2009) and ImageNet (Deng et al., 2009).

**CIFAR.** The CIFAR dataset consists of 60k colored images with a resolution of  $32 \times 32$ . The images are separated into 50k training samples and 10k test samples. There are 10 classes of objects in CIFAR-10 and 100 classes of objects in CIFAR-100. We apply the same data preprocessing for CIFAR-10 and CIFAR-100, which contains data normalization, random horizontal flipping, cutout (DeVries and Taylor, 2017), and random cropping. We employ direct encoding (Rathi and Roy, 2021) to convert image pixels into time series. In this method, the floating-point pixel matrix of the images is duplicated at each time step and then fed into the first layer of the SNN architecture.

**ImageNet.** The ImageNet dataset consists of over 1250k training images, 50k validation images, and 100k test images. We apply data normalization so that the input data have zero mean and unit variance. Besides, our data preprocessing contains random resized cropping and horizontal flipping. The input size is set to  $224 \times 224$  by default. We also use the direct encoding (Rathi and Roy, 2021), as done for the CIFAR dataset.

Dataset	CIFAR-10	CIFAR-100	ImageNet
Optimizer	SGD	SGD	SGD
Epoch	300	300	120
$lr$	0.1	0.1	0.1
$lr$ scheduler	Cosine Annealing	Cosine Annealing	Cosine Annealing
Weight decay	1e-4	1e-4	4e-5
Batch size per GPU	64	64	16
GPU	1	1	16

Table B.6: Hyperparameters for training on CIFAR-10/100 and ImageNet.

## 485 Appendix B.2. Training Settings

Our implementation is based on PyTorch (Paszke et al., 2019). We use SpikingJelly (Fang et al., 2020) to implement the LIF neuron. Specifically, we set  $\lambda = 3.0$ ,  $V_{reset} = 0$ , and  $V_{th} = 1$  in every spiking neuron for all datasets. The surrogate gradient used in this work can be formulated as

$$\frac{\partial S^l[t]}{\partial H^l[t]} = \frac{\alpha}{2 \left[ 1 + \left( \frac{\pi}{2} \alpha H^l[t] \right)^2 \right]}, \quad (\text{B.1})$$

490 where we set  $\alpha = 2$  for all datasets. We use the cross-entropy loss and adopt the standard STBP (Wu et al., 2018) training framework to train the SNN architecture. As recommended by (Zenke and Vogels, 2021), We detach the computational graph of reset during backpropagation to further improve the performance.

495 The hyperparameters about optimization are shown in Table B.6. We use an SGD optimizer (Rumelhart et al., 1986) with momentum 0.9 to train

our models in all experiments. The weight decay is set to 1e-4 and 4e-5 for CIFAR-10/100 and ImageNet, respectively. We set the initial learning rate to 0.1 for all datasets and use a cosine learning rate decay (Loshchilov and  
500 Hutter, 2017). We adopt the mixed precision training (Micikevicius et al., 2018) in order to reduce memory consumption and speed up our training process. For the ImageNet dataset, we train our model on multi-GPU, and we use the synchronized batch normalization (SyncBN) (Zhang et al., 2018) technique.

505 The experiments are conducted on NVIDIA Tesla A100 GPU or NVIDIA GeForce RTX 3090 GPU.

## Appendix C. Energy Consumption Analysis Details

We conduct an energy consumption analysis following previous studies (Li et al., 2021; Che et al., 2022; Deng et al., 2022). Before calculating  
510 the theoretical energy consumption, we calculate the number of synaptic operations in SNNs. This calculation is performed as follows:

$$SOP^l = fr \times T \times FLOPs^l, \quad (C.1)$$

where  $l$  represents a layer,  $SOP^l$  denotes the number of synaptic operations in layer  $l$ ,  $fr$  represents the average firing rate of the layer,  $T$  denotes the number of time steps,  $FLOPs^l$  refers to the number of floating point operations of  
515 the layer.

Regarding our architecture, the first layer performs multiply-and-accumulate (MAC) operations since it receives non-binary inputs. In all subsequent layers, the architecture transfers spikes and performs accumulate (AC) operations. Therefore, we can quantify the estimated energy consumption of our



520 architecture, denoted as  $E_{TANet}$ , as follows:

$$E_{TANet} = E_{MAC} \cdot FLOPs^1 + E_{AC} \cdot \sum_{n=2}^N SOP^n, \quad (C.2)$$

where  $N$  is the total number of layers,  $E_{MAC}$  and  $E_{AC}$  represent the energy cost of MAC and AC operation, respectively.  $FLOPs^1$  denotes the number of floating point operations in the first layer. Refer to previous studies (Li et al., 2021; Che et al., 2022), we assume that the data for various operations are  
 525 32-bit floating-point implementation in 45nm technology (Horowitz, 2014), with  $E_{MAC} = 4.6pJ$  and  $E_{AC} = 0.9pJ$ .

## References

- Albert, R. and Barabási, A.-L. (2002). Statistical mechanics of complex networks. *Reviews of Modern Physics*, 74(1):47.
- 530 Bender, G., Kindermans, P.-J., Zoph, B., Vasudevan, V., and Le, Q. (2018). Understanding and simplifying one-shot architecture search. In *International Conference on Machine Learning*.
- Bu, T., Fang, W., Ding, J., Dai, P., Yu, Z., and Huang, T. (2022). Optimal ANN-SNN conversion for high-accuracy and ultra-low-latency spiking  
 535 neural networks. In *International Conference on Learning Representations*.
- Cai, H., Gan, C., Wang, T., Zhang, Z., and Han, S. (2019). Once-for-all: Train one network and specialize it for efficient deployment. *arXiv preprint arXiv:1908.09791*.

- 540 Che, K., Leng, L., Zhang, K., Zhang, J., Meng, Q., Cheng, J., Guo, Q.,  
and Liao, J. (2022). Differentiable hierarchical and surrogate gradient  
search for spiking neural networks. In *Advances in Neural Information  
Processing Systems*.
- Chollet, F. (2017). Xception: Deep learning with depthwise separable con-  
545 volutions. In *Proceedings of the IEEE Conference on Computer Vision  
and Pattern Recognition*.
- Deng, J., Dong, W., Socher, R., Li, L.-J., Li, K., and Fei-Fei, L. (2009).  
Imagenet: A large-scale hierarchical image database. In *Proceedings of  
the IEEE Conference on Computer Vision and Pattern Recognition*.
- 550 Deng, S., Li, Y., Zhang, S., and Gu, S. (2022). Temporal efficient training  
of spiking neural network via gradient re-weighting. In *International  
Conference on Learning Representations*.
- DeVries, T. and Taylor, G. W. (2017). Improved regularization of convolu-  
tional neural networks with cutout. *arXiv preprint arXiv:1708.04552*.
- 555 Dong, X. and Yang, Y. (2019). Searching for a robust neural architecture  
in four gpu hours. In *Proceedings of the IEEE Conference on Computer  
Vision and Pattern Recognition*.
- Dong, X. and Yang, Y. (2020). NAS-Bench-201: Extending the scope of  
reproducible neural architecture search. In *International Conference on  
560 Learning Representations*.
- Fang, W., Chen, Y., Ding, J., Chen, D., Yu, Z., Zhou, H., Tian, Y.,

and other contributors (2020). Spikingjelly. <https://github.com/fangwei123456/spikingjelly>.

Fang, W., Yu, Z., Chen, Y., Huang, T., Masquelier, T., and Tian, Y. (2021a).  
565 Deep residual learning in spiking neural networks. In *Advances in Neural  
Information Processing Systems*.

Fang, W., Yu, Z., Chen, Y., Masquelier, T., Huang, T., and Tian, Y. (2021b).  
Incorporating learnable membrane time constant to enhance learning of  
spiking neural networks. In *Proceedings of the IEEE/CVF International  
570 Conference on Computer Vision*.

Guo, Z., Zhang, X., Mu, H., Heng, W., Liu, Z., Wei, Y., and Sun, J. (2020).  
Single path one-shot neural architecture search with uniform sampling.  
In *Proceedings of the European Conference on Computer Vision*.

Han, B., Srinivasan, G., and Roy, K. (2020). RMP-SNN: Residual membrane  
575 potential neuron for enabling deeper high-accuracy and low-latency spik-  
ing neural network. In *Proceedings of the IEEE Conference on Computer  
Vision and Pattern Recognition*.

He, K., Zhang, X., Ren, S., and Sun, J. (2016). Deep residual learning for  
image recognition. In *Proceedings of the IEEE Conference on Computer  
580 Vision and Pattern Recognition*.

Horowitz, M. (2014). 1.1 computing’s energy problem (and what we can do  
about it). In *2014 IEEE International Solid-State Circuits Conference  
Digest of Technical Papers (ISSCC)*, pages 10–14. IEEE.

- Kim, S., Park, S., Na, B., and Yoon, S. (2020). Spiking-yolo: Spiking neural  
585 network for energy-efficient object detection. In *Proceedings of the AAAI Conference on Artificial Intelligence*.
- Kim, Y., Li, Y., Park, H., Venkatesha, Y., and Panda, P. (2022). Neural  
architecture search for spiking neural networks. In *Proceedings of the European Conference on Computer Vision*.
- 590 Krizhevsky, A., Hinton, G., et al. (2009). Learning multiple layers of features from tiny images. *Tech Report*.
- Kugele, A., Pfeil, T., Pfeiffer, M., and Chicca, E. (2020). Efficient processing of spatio-temporal data streams with spiking neural networks. *Frontiers in Neuroscience*, 14:439.
- 595 Lee, J. H., Delbruck, T., and Pfeiffer, M. (2016). Training deep spiking neural networks using backpropagation. *Frontiers in Neuroscience*, 10:508.
- Li, L. and Talwalkar, A. (2019). Random search and reproducibility for neural architecture search. In *Uncertainty in Artificial Intelligence*.
- Li, Y., Guo, Y., Zhang, S., Deng, S., Hai, Y., and Gu, S. (2021). Differentiable  
600 spike: Rethinking gradient-descent for training spiking neural networks. In *Advances in Neural Information Processing Systems*.
- Liu, H., Simonyan, K., and Yang, Y. (2019). DARTS: Differentiable architecture search. In *International Conference on Learning Representations*.
- Loshchilov, I. and Hutter, F. (2017). Sgdr: Stochastic gradient descent with  
605 warm restarts. In *International Conference on Learning Representations*.

- Maass, W. (1997). Networks of spiking neurons: the third generation of neural network models. *Neural Networks*, 10(9):1659–1671.
- Meng, Q., Xiao, M., Yan, S., Wang, Y., Lin, Z., and Luo, Z.-Q. (2022). Training high-performance low-latency spiking neural networks by differentiation on spike representation. In *Proceedings of the IEEE Conference on Computer Vision and Pattern Recognition*.  
610
- Micikevicius, P., Narang, S., Alben, J., Diamos, G., Elsen, E., Garcia, D., Ginsburg, B., Houston, M., Kuchaiev, O., Venkatesh, G., et al. (2018). Mixed precision training. In *International Conference on Learning Representations*.  
615
- Na, B., Mok, J., Park, S., Lee, D., Choe, H., and Yoon, S. (2022). AutoSNN: Towards energy-efficient spiking neural networks. In *International Conference on Machine Learning*.
- Orchard, G., Frady, E. P., Rubin, D. B. D., Sanborn, S., Shrestha, S. B., Sommer, F. T., and Davies, M. (2021). Efficient neuromorphic signal processing with loihi 2. In *2021 IEEE Workshop on Signal Processing Systems (SiPS)*.  
620
- Paszke, A., Gross, S., Massa, F., Lerer, A., Bradbury, J., Chanan, G., Killeen, T., Lin, Z., Gimelshein, N., Antiga, L., et al. (2019). Pytorch: An imperative style, high-performance deep learning library. In *Advances in Neural Information Processing Systems*.  
625
- Patel, K., Hunsberger, E., Batir, S., and Eliasmith, C. (2021). A spiking neural network for image segmentation. *arXiv preprint arXiv:2106.08921*.

- Pham, H., Guan, M., Zoph, B., Le, Q., and Dean, J. (2018). Efficient neural  
630 architecture search via parameters sharing. In *International Conference on Machine Learning*.
- Rathi, N. and Roy, K. (2021). Diet-SNN: A low-latency spiking neural network with direct input encoding and leakage and threshold optimization. *IEEE Transactions on Neural Networks and Learning Systems*.
- 635 Rathi, N., Srinivasan, G., Panda, P., and Roy, K. (2020). Enabling deep spiking neural networks with hybrid conversion and spike timing dependent backpropagation. In *International Conference on Learning Representations*.
- Roy, K., Jaiswal, A., and Panda, P. (2019). Towards spike-based machine  
640 intelligence with neuromorphic computing. *Nature*, 575(7784):607–617.
- Rueckauer, B., Lungu, I.-A., Hu, Y., Pfeiffer, M., and Liu, S.-C. (2017). Conversion of continuous-valued deep networks to efficient event-driven networks for image classification. *Frontiers in Neuroscience*, 11:682.
- Rumelhart, D. E., Hinton, G. E., and Williams, R. J. (1986). Learning  
645 representations by back-propagating errors. *Nature*, 323(6088):533–536.
- Sciuto, C., Yu, K., Jaggi, M., Musat, C., and Salzmann, M. (2020). Evaluating the search phase of neural architecture search. In *International Conference on Learning Representations*.
- Shrestha, S. B. and Orchard, G. (2018). Slayer: Spike layer error reassignment in time. In *Advances in Neural Information Processing Systems*.  
650

- Simonyan, K. and Zisserman, A. (2015). Very deep convolutional networks for large-scale image recognition. In *International Conference on Learning Representations*.
- 655 Srivastava, N., Hinton, G., Krizhevsky, A., Sutskever, I., and Salakhutdinov, R. (2014). Dropout: a simple way to prevent neural networks from overfitting. *The Journal of Machine Learning Research*, 15(1):1929–1958.
- Watts, D. J. and Strogatz, S. H. (1998). Collective dynamics of ‘small-world’ networks. *Nature*, 393(6684):440–442.
- 660 Wu, B., Dai, X., Zhang, P., Wang, Y., Sun, F., Wu, Y., Tian, Y., Vajda, P., Jia, Y., and Keutzer, K. (2019). Fbnet: Hardware-aware efficient convnet design via differentiable neural architecture search. In *Proceedings of the IEEE Conference on Computer Vision and Pattern Recognition*.
- 665 Wu, Y., Deng, L., Li, G., Zhu, J., and Shi, L. (2018). Spatio-temporal backpropagation for training high-performance spiking neural networks. *Frontiers in Neuroscience*, 12:331.
- Xiao, M., Meng, Q., Zhang, Z., Wang, Y., and Lin, Z. (2021). Training feedback spiking neural networks by implicit differentiation on the equilibrium state. In *Advances in Neural Information Processing Systems*.
- 670 Xie, S., Kirillov, A., Girshick, R., and He, K. (2019). Exploring randomly wired neural networks for image recognition. In *Proceedings of the IEEE/CVF International Conference on Computer Vision*.

- Yan, Z., Zhou, J., and Wong, W.-F. (2021). Near lossless transfer learning for spiking neural networks. In *Proceedings of the AAAI Conference on Artificial Intelligence*.  
675
- Zenke, F. and Vogels, T. P. (2021). The remarkable robustness of surrogate gradient learning for instilling complex function in spiking neural networks. *Neural Computation*, 33(4):899–925.
- Zhang, H., Dana, K., Shi, J., Zhang, Z., Wang, X., Tyagi, A., and Agrawal, A. (2018). Context encoding for semantic segmentation. In *Proceedings of the IEEE Conference on Computer Vision and Pattern Recognition*.  
680
- Zheng, H., Wu, Y., Deng, L., Hu, Y., and Li, G. (2021). Going deeper with directly-trained larger spiking neural networks. In *Proceedings of the AAAI Conference on Artificial Intelligence*.
- 685 Zoph, B. and Le, Q. V. (2017). Neural architecture search with reinforcement learning. In *International Conference on Learning Representations*.
- Zoph, B., Vasudevan, V., Shlens, J., and Le, Q. V. (2018). Learning transferable architectures for scalable image recognition. In *Proceedings of the IEEE Conference on Computer Vision and Pattern Recognition*.